Experimental investigation and parametric analysis of a solar thermal dish collector with spiral absorber

Sasa Pavlovic[a], Evangelos Bellos[b], Willem G. Le Roux[c], Velimir Stefanovic[a], Christos Tzivanidis[b]

[a]Department of Energetics and Process Technique, Faculty of Mechanical Engineering, University in Niš, Serbia

[b]Department of Mechanical Engineering, National Technical University of Athens, Zografou, Heroon Polytechniou 9, 15780 Athens, Greece

[c]Department of Mechanical and Aeronautical Engineering, University of Pretoria, Pretoria, South Africa

Corresponding author: Evangelos Bellos (bellose@central.ntua.gr)

Highlights

- A solar dish collector with spiral absorber is investigated experimentally.
- A thermal model developed in EES is validated with experimental results.
- Water, thermal oil and air are examined at various mass flow rates and temperatures.
- Maximum exergetic efficiency is 7.58% for thermal oil at inlet temperature of 155 °C.
- System is feasible where solar potential is 1600 kW h/m^2 and heating cost 0.15 €/kW h.

Abstract

Solar-tracking dish collectors are a potential alternative to fossil fuels because of their high concentration ratios. Important considerations for solar collectors are manufacturing costs, complexity, efficiency, uniform flux distribution and working fluid selection. In this study, a simple, low-cost solar dish collector with a spiral absorber and lightweight structure is examined. Experiments were performed with water as working fluid where the volumetric flow rate, inlet and outlet temperatures, ambient temperature, air velocity and solar irradiation were measured. Experimental results were used to validate a numerical model developed in Engineering Equation Solver, where three working fluids (water, thermal oil and air) were considered in various operating conditions. According to the thermal analysis, water is the most appropriate working fluid for low-temperature applications and thermal oil the most appropriate for higher-temperature applications. The exergetic analysis, however, shows that air is the most appropriate for low-temperature applications

and thermal oil the most appropriate for higher-temperature applications. The highest exergetic efficiency was observed for thermal oil with inlet temperature of 155 ^{o}C. The system can be feasible in areas with solar potential of more than 1600 kWh/m^2 and where the cost of heating is more than 0.15 €/kWh.

Keywords
Dish, exergetic efficiency, solar collector, spiral, absorber

1. Introduction

Energy plays a pivotal role in our society because of new life trends which are accompanied with high energy consumption [1]. Moreover, there are many important problems related to the energy domain, such as increasing electricity demand, high CO_2 emissions, fossil fuel depletion and irrigation problems [2-7]. As an alternative to fossil fuels, renewable and alternative energy sources can be sustainable, cheap and abundant. Solar energy utilization is a key solution to energy problems, giving efficient, clean and financially viable solutions [8]. Moreover, the use of new and innovative techniques in the design of energy systems is vital for making the use of renewable energy sources financially feasible [9-10].

Solar collectors capture solar energy and transform it to useful heat, with satisfying efficiency. Selection of the most suitable collector type is dictated by the inlet temperature, and the findings in the literature are: (a) at applications of up to 100 ^{o}C, flat plate collectors are used [11]; (b) between 100 ^{o}C and 200 ^{o}C, evacuated collectors and collectors with low concentration ratios are used (<5) [12]; and (c) above 200 ^{o}C, parabolic trough collectors are used [13]. Abid et al. [14] compared a solar dish collector with a parabolic trough collector and showed that the dish technology performs better energetically and exergetically. The main reason for this result is that higher concentration ratios are associated with lower thermal losses and higher thermal efficiency.

Solar dish collectors have been used in a great variety of applications such as heat generation, electricity generation [15-19] and desalination systems [20-21]. Le Roux et al. [15] showed that an open-cavity tubular solar receiver can be used for a small-scale dish-mounted solar thermal Brayton cycle. Loni et al. [16-17] also considered the use of a solar dish collector with tubular cavity receiver for an organic Rankine cycle. The conjugation of Stirling heat engines with solar dish collectors is also a promising technology for generating electricity with a high efficiency, but it also has a high investment cost [18]. Recent studies in this research field aim to reduce the cost of the system and to design collectors with higher optical performance. Li et al. [19] utilized a Monte-Carlo ray tracing method for determining the heat flux distribution over the receiver in a solar dish Stirling power facility. The results proved that the most uniform heat flux profile can be achieved with a shallow semi-ellipsoidal receiver.

Much research has been focused on the optimization of the receiver in solar dish collectors, showing that there is a compromise between manufacturing costs, complexity, efficiency and uniform flux distribution. Various configurations have been suggested and analyzed in recent literature and experimental studies have also been performed. In a recent study, Daabo et al. [22] examined three receiver geometries: a cylinder, a cone and a sphere. In each case, a helical tube was used in order to utilize the captured solar energy efficiently. It was found that the conical shape is the best choice. Moreover, they proved that the optimum reflector geometry is dependent on the selected receiver; an interesting result which is useful in the design of innovative solar dish collectors. Zhu et al. [23] examined a pressurized volumetric receiver in a solar dish system which leads to high thermal efficiency, but this configuration is very complex.

In this study, a simple, low-cost solar dish collector with a spiral absorber and lightweight structure is examined. A spiral absorber is easily manufactured and the solar irradiation distribution profile over its surface tends to be uniform. The configuration of the collector is described in Section 2. Experimental results of the collector are compared with results of a numerical model developed in EES (Engineering Equation Solver). The numerical model is used for the parametric analysis of the dish performance with air, water and thermal oil. The lack of studies which examine liquid and gas working fluids under the same operating conditions makes this work notable. The optimum volumetric flow rate for each working fluid is determined from an energetic and exergetic sensitivity analysis. The final results of this study can be used to determine the operating conditions of this collector in applications such as solar heating and cooling, power generation, cogeneration and trigeneration. Moreover, a simple parametric financial evaluation of the examined system is also presented.

2. Description of collector setup

The examined collector is a concentrating collector with dish reflector. The collector is shown in Figure 1 where the main parts are indicated. The solar dish reflector consists of 11 curvilinear trapezoidal reflective petals constructed of PMMA (Polymethyl methacrylate) with a silvered mirror layer. The 12th part of the reflector is missing in order to accommodate the bracket which supports the system. The stainless steel absorber is a corrugated spiral tube which is located inside an aluminum housing.

The collector has been created from low-cost materials in order to reduce the total investment cost, while sufficient performance is maintained. The total cost of the system was about 7000 €. The tracking system cost about 2000 €, reflectors approximately 2000 € and the other parts about 3000 €. Apart from the low cost, this collector also has a lightweight construction and is relatively easy to install.

Table 1 summarizes the geometric characteristics as well as the thermal and optical properties. The final reflectance was estimated to be about 60%. This value was selected due to dust and some stains on the mirrors. While the absorber tube is not selective, thus

having high emittance, its low cost is an advantage. More details on the system geometry can be found in Ref. [24].

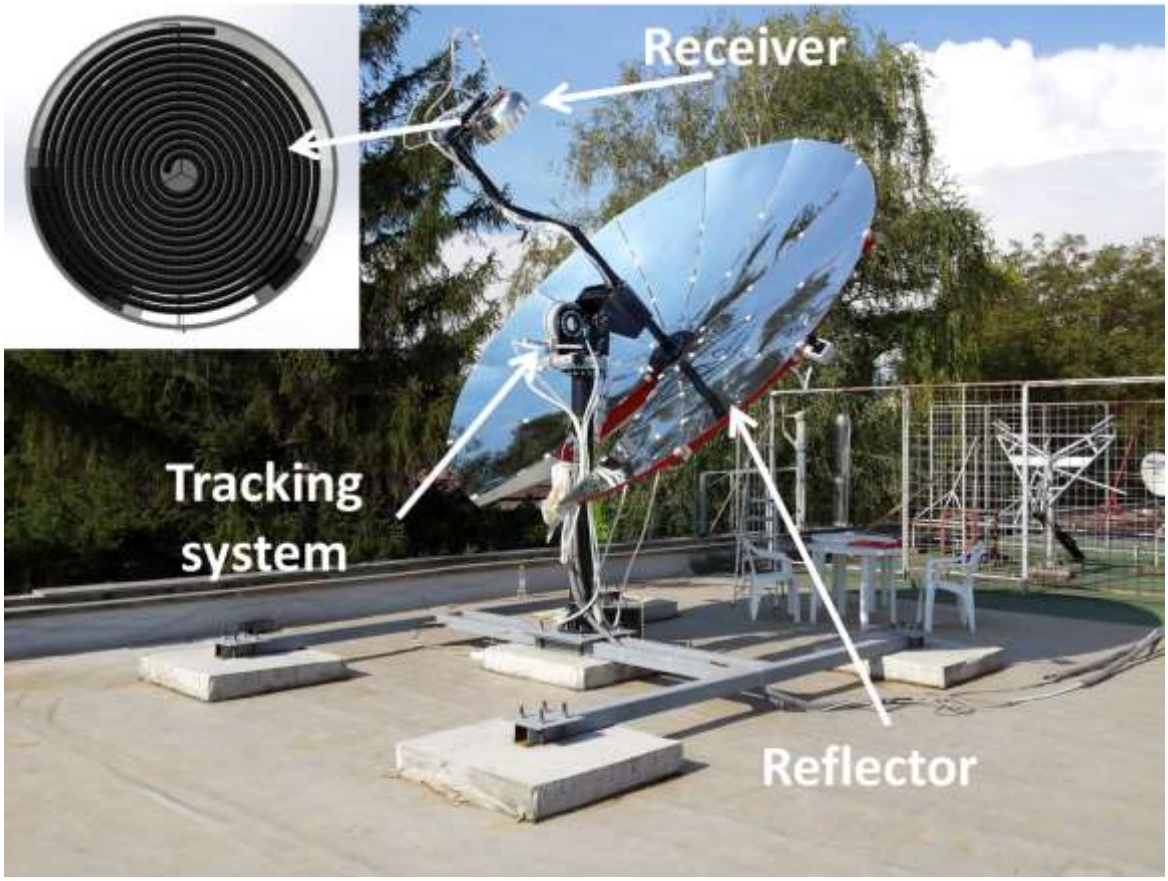

Figure 1. The examined solar dish collector

Table 1. Basic parameters of the examined collector

Parameter	Value
Concentration ratio	28.26
Concentrator diameter	3.80 m
Paraboloid rim angle	45.6 ^{o}
Focal distance	2.26 m
Collector aperture	10.29 m^2
Spiral length	9.5 m
Spiral outer mean diameter	12.2 mm
Spiral inner maximum diameter	11.7 mm
Spiral inner mean diameter	10.5 mm
Spiral inner minimum diameter	9.3 mm
Absorber emittance	0.9
Absorber absorbance	0.9
Mirror reflectance	0.6
Distance between absorber and reflector base	2.1 m

3. Mathematical modelling

The model equations are presented here. As an acceptable simplification, uniform flux over the absorber is assumed.

3.1 Solar irradiation utilization

Concentrating collectors with high concentration ratios, as in the examined case, utilize only the direct beam solar irradiation and the available solar heat rate is calculated as the product of the effective dish aperture and the beam irradiation:

$$Q_s = A_a \cdot G_b, \tag{1}$$

The concentration ratio of the collector is the ratio of the available aperture to the receiver area:

$$C = \frac{A_a}{A_r}, \tag{2}$$

The absorbed heat rate of the receiver can be calculated using the optical efficiency of the collector (η_{opt}):

$$Q_{abs} = \eta_{opt} \cdot Q_s, \tag{3}$$

3.2 Thermal analysis

The developed thermal analysis model is based on the energy balance in the receiver. The absorbed solar irradiation is divided into useful energy and thermal losses to the environment, as:

$$Q_{abs} = Q_u + Q_{loss}, \tag{4}$$

The useful heat output rate can be calculated by the energy balance in the fluid volume as:

$$Q_u = m \cdot c_p \cdot \left(T_{out} - T_{in}\right), \tag{5}$$

The thermal losses consist of radiation and convection heat losses:

$$Q_{rad} = A_{ro} \cdot \varepsilon_r \cdot \sigma \cdot \left(T_r^4 - T_{am}^4\right), \tag{6}$$

$$Q_{conv} = A_{ro} \cdot h_{air} \cdot \left(T_r - T_{am}\right), \tag{7}$$

The convection heat transfer coefficient between absorber and ambient can be estimated by the following equation [25]:

$$h_{air} = 2.8 + 3 \cdot V_{air}, \tag{8}$$

The thermal efficiency of the collector is calculated as the ratio of the useful heat rate to the available solar irradiation:

$$\eta_{th} = \frac{Q_u}{Q_s}, \tag{9}$$

3.3 Heat transfer in the flow

In this section, the equations related to the heat transfer from the absorber to the fluid are presented. The useful heat transfer rate that the fluid gains can be calculated as:

$$Q_u = h \cdot A_{ri} \cdot \left(T_r - T_{fm}\right), \tag{10}$$

The mean fluid temperature can be approximated by the following equation:

$$T_{fm} = \frac{T_{in} + T_{out}}{2}, \tag{11}$$

The heat transfer coefficient for the examined case is calculated according to Equation 12 [26]. This formula is used for turbulent flow with Reynolds number over 2300, as is the case in the present study.

$$Nu = \frac{\left(\frac{f_r}{8}\right) \cdot \mathrm{Re} \cdot \mathrm{Pr}}{1 + 12.8 \cdot \sqrt{\frac{f_r}{8}} \cdot \left(\mathrm{Pr}^{0.68} - 1\right)}, \tag{12}$$

The friction factor has to be determined by a complex equation because a corrugated tube is used. The following equation is suitable for the examined case [27]:

$$f_r = 0.316 \cdot \mathrm{Re}^{-0.25} + 0.41 \cdot \left(\frac{D_{ri,\min}}{D_{ri}}\right)^{0.9}, \tag{13}$$

It is important to state that the mean internal diameter is the diameter that is used for Reynolds definition. The following equations present the characteristic numbers of Reynolds, Prandtl and Nusselt:

$$\mathrm{Re} = \frac{4 \cdot m}{\pi \cdot D_{ri} \cdot \mu}, \tag{14}$$

$$\mathrm{Pr} = \frac{\mu \cdot c_p}{k}, \tag{15}$$

$$Nu = \frac{h \cdot D_{ri}}{k}, \tag{16}$$

The last important parameter for this study is the pressure drop along the tube, calculated according to the friction factor:

$$\Delta P = f_r \cdot \frac{L}{D_{ri}} \cdot \left(\frac{1}{2} \cdot \rho \cdot u^2 \right), \tag{17}$$

The flow velocity is calculated from the mass flow rate:

$$u = \frac{m}{\left(\frac{\pi}{4} \cdot D_{ri}^2 \right) \cdot \rho}, \tag{18}$$

3.4 Exergetic performance

The exergetic (or second law) evaluation of the solar collector is a useful analysis which shows the quality of the process. In the exergetic analysis, the thermal performance and the operating temperatures are taken into account, as well as the pressure drop in the tube. The useful exergy output rate is equal to the exergy transfer rate by heat minus the irreversibility rate of the heating process. The following equation shows that the irreversibility rate can be expressed via the specific entropy increase:

$$E_u = Q_u \left(1 - \frac{T_{am}}{T_r} \right) - T_{am} \left(m \cdot \Delta s - \frac{Q_u}{T_r} \right), \tag{19}$$

This equation can be transformed to the following formula [28]:

$$E_u = Q_u - m \cdot c_p \cdot T_{am} \cdot \ln \left[\frac{T_{out}}{T_{in}} \right] - m \cdot T_{am} \frac{\Delta P}{\rho \cdot T_{fm}}, \tag{20}$$

The exergy rate of the solar irradiation is calculated by the Petela model. The sun is not a heat reservoir but a radiation reservoir and for this reason there is an extra term in the following equation [29].

$$E_s = Q_s \cdot \left[1 - \frac{4}{3} \cdot \left(\frac{T_{am}}{T_{sun}} \right) + \frac{1}{3} \cdot \left(\frac{T_{am}}{T_{sun}} \right)^4 \right], \tag{21}$$

The sun's temperature can be estimated as 5770K, which is a mean value of the outer surface temperature of the sun. Note that the temperatures in Equations 20 and 21 have to be in degrees Kelvin. The exergetic efficiency of the solar collector is defined as the ratio of the useful exergy output rate to the solar exergy input rate. This parameter is calculated as follows [29]:

$$\eta_{ex} = \frac{E_u}{E_s}, \tag{22}$$

4. Methodology

In this section, the experimentally established energetic and exergetic performance of the collector are presented for a sunny day. The experimental results are then compared to those obtained with a 1-D model developed by the authors. After validating this model, the collector is further investigated numerically for additional operating conditions. More specifically, three working fluids (water, thermal oil and air) are investigated for various flow rates and fluid inlet temperatures. These fluids are compared energetically and exergetically for their optimum flow rates.

4.1 Experimental setup

The experimental setup has been installed at the solar laboratory of the Faculty of Mechanical Engineering in Nis (latitude $43^o19'$ and longitude $21^o54'$). The solar dish collector was connected to a water storage tank of 500 litres. Experiments were performed between the end of August 2016 and the beginning of September 2016. The following parameters were measured: the volumetric water flow rate (V) with a flowmeter, the water inlet temperature, water outlet temperature and ambient temperature with thermometers (PT100) and the air velocity. A solar tracking system was used to ensure that sun rays are normal to the dish aperture. The direct normal solar beam irradiation was determined by two pyranometers mounted on the solar tracking system that measured the global (G) and the diffuse (G_d) solar irradiation. A time step of 30 seconds was used. Water mass flow rate, direct normal solar beam irradiation, thermal efficiency and exergetic efficiency are given by the following equations. Note that in Equation 26, the temperatures have to be in degrees Kelvin.

$$m(kg/s) = \frac{\rho(kg/m^3)\cdot V(l/h)}{1000(l/m^3)\cdot 3600(s/h)}, \tag{23}$$

$$G_b = G - G_d, \tag{24}$$

$$\eta_{th} = \frac{m\cdot c_p\cdot(T_{out}-T_{in})}{A_a\cdot G_b}, \tag{25}$$

$$\eta_{ex} = \frac{m\cdot c_p\cdot(T_{out}-T_{in}) - m\cdot c_p\cdot T_{am}\cdot\ln\left[\frac{T_{out}}{T_{in}}\right] - m\cdot T_{am}\frac{\Delta P}{\rho\cdot T_{fm}}}{A_a\cdot G_b\cdot\left[1-\frac{4}{3}\cdot\left(\frac{T_{am}}{T_{sun}}\right)+\frac{1}{3}\cdot\left(\frac{T_{am}}{T_{sun}}\right)^4\right]}, \tag{26}$$

The intercept factor (γ) of the system was estimated to be 65%, after taking into account manufacturing errors in the system design, due to its low construction cost. The optical efficiency is calculated according to the following equation:

$$\eta_{opt} = \rho_c\cdot\alpha\cdot\gamma = 0.6\cdot 0.9\cdot 0.65 = 0.35, \tag{27}$$

This result is used in the numerical model described in the next section.

4.2 Numerical model

The developed numerical model is a 1-D thermal model which is based on the energy balance of the absorber. The average absorber temperature is the key unknown which has to be calculated in each case. This strategy has also been followed in Ref. [28] and is a validated method for concentrating solar collectors. The calculations have been carried out with EES (Engineering Equation Solver) [30]. The properties of water, thermal oil (Therminol VP-1) and air have been taken from the EES library [31-33]. It is essential to note that inlet temperatures of up to 85 ^{o}C were considered for water and inlet temperatures of up to 300 ^{o}C were considered for Therminol VP-1 and air.

A simple strategy has been followed for the validation of the numerical model from the experimental results. More specifically, many operating points have been selected and in each case the water outlet temperature and the thermal efficiency were compared. For each examined case, the water inlet temperature, the solar beam irradiation, the volumetric flow rate, the ambient temperature and the air velocity were inserted in the numerical model in order to simulate the respective real conditions of the experiment. The outlet temperature is the most important parameter because it is associated with the useful heat and the thermal efficiency.

5. Results

In this section, the experimental and numerical results are presented. Section 5.1 includes the experimental results and the validation of the developed numerical model. Sections 5.2 and 5.3 are dedicated to the numerical investigation of the optimum flow rate and performance of various working fluids. Energetic and financial assessments of the collector are presented in Section 5.4.

5.1 Experimental results and validation

In this section, experimental and numerical results are presented and compared. The collector was examined over a number of days. The 3rd of September 2016 was selected because of stable solar irradiation (Table 2 and Figure 2).

Water outlet temperature is a key experimental parameter since it is needed for the calculation of energy and thermal efficiency. Figure 3 shows a very good match between the measured and calculated outlet temperature. It is interesting to note that the outlet temperature increased during the collector operation because the inlet temperature also increased. The storage tank aids the system to store energy and to operate at higher temperatures.

The thermal efficiency and the exergetic efficiency are depicted in Figures 4 and 5 respectively. According to Figure 4, the thermal efficiency of the collector is about 34%. This low value is explained by the low optical performance (η_{opt}), as was also mentioned in Section 4. The exergetic efficiency, which is shown in Figure 5, is lower than 2.5% because of the low operating temperatures of the collector.

The average receiver and fluid temperatures are shown in Figure 6. The results are calculated numerically for all the examined cases. These temperatures are close to each other because of the high convection heat transfer coefficient, which is also shown in the same figure. The high values of this coefficient are explained by the corrugated tube which creates turbulent flow conditions.

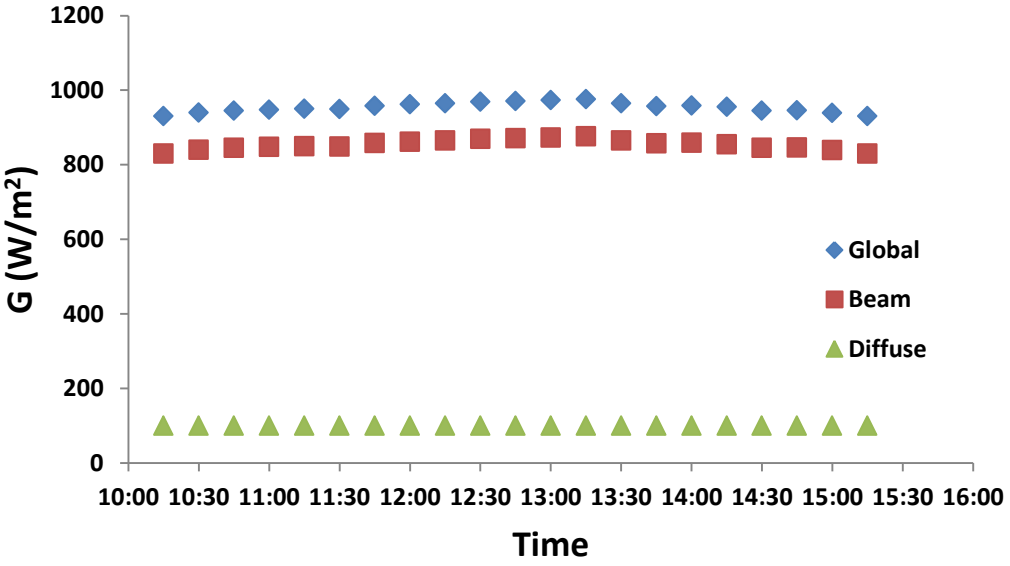

Figure 2. Solar irradiation for the examined day

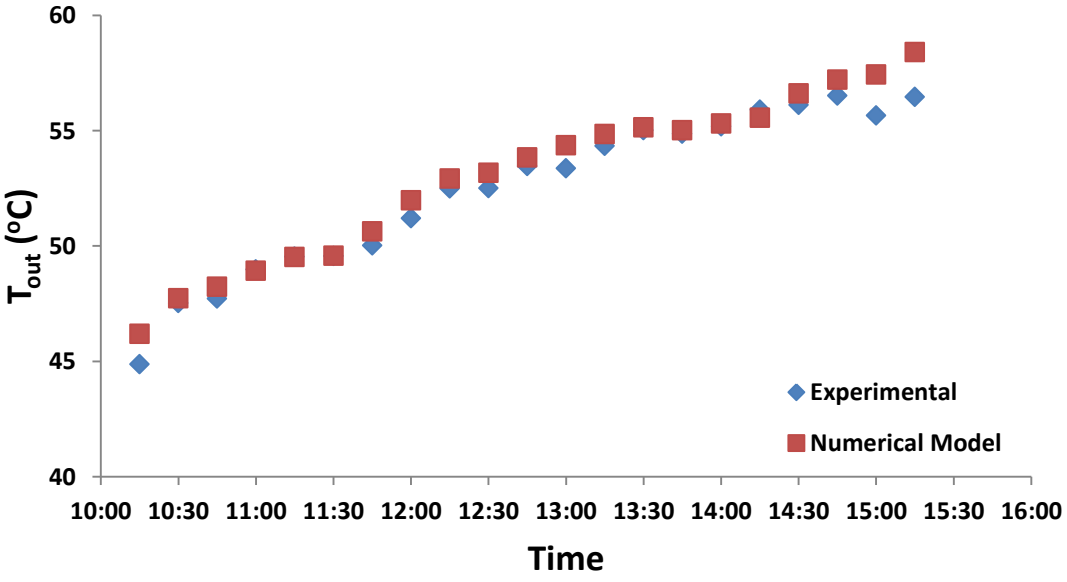

Figure 3. Water outlet temperature for the examined day

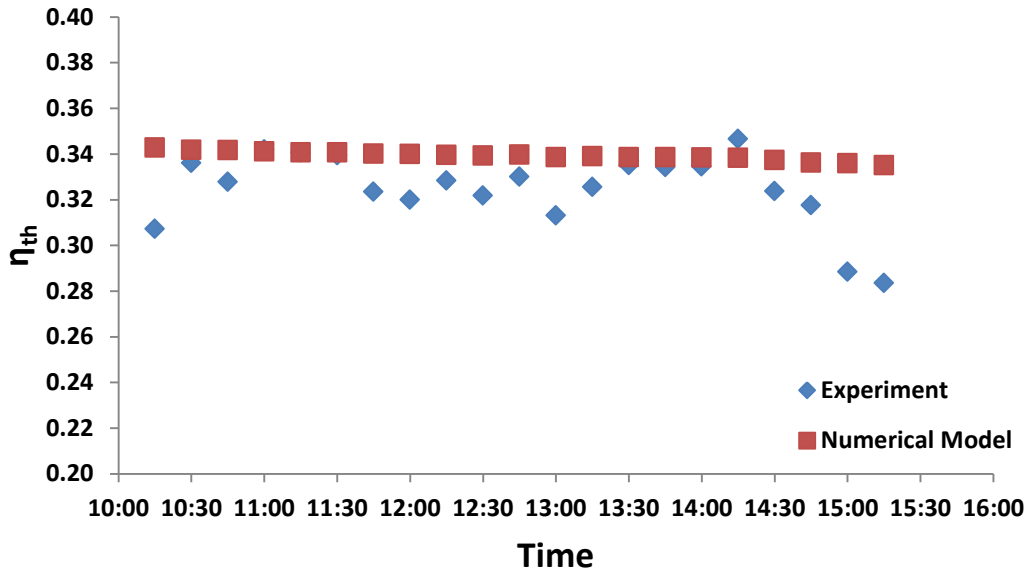

Figure 4. Thermal efficiency for the examined day

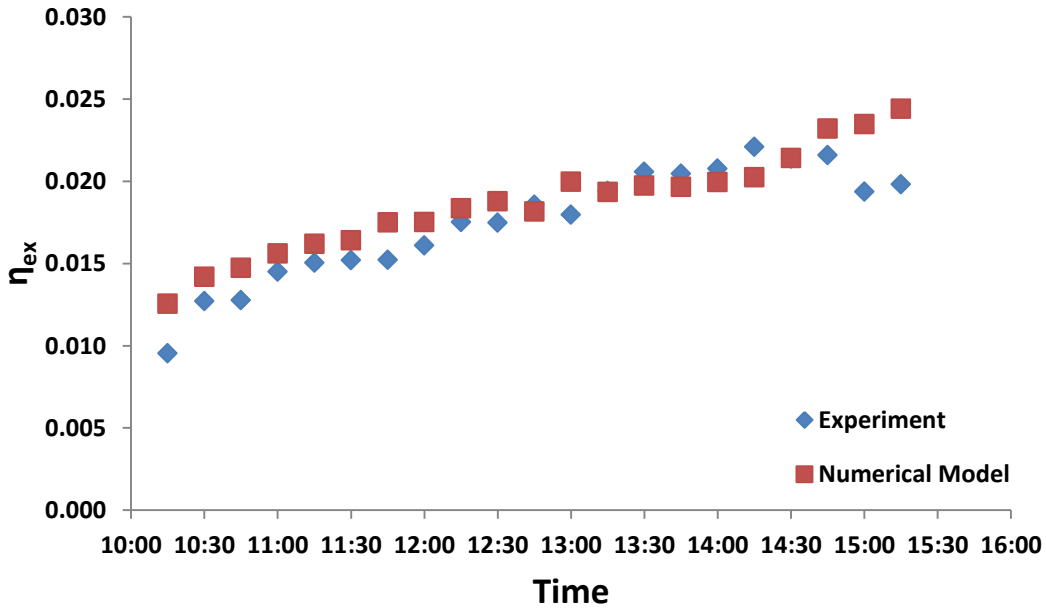

Figure 5. Exergetic efficiency for the examined day

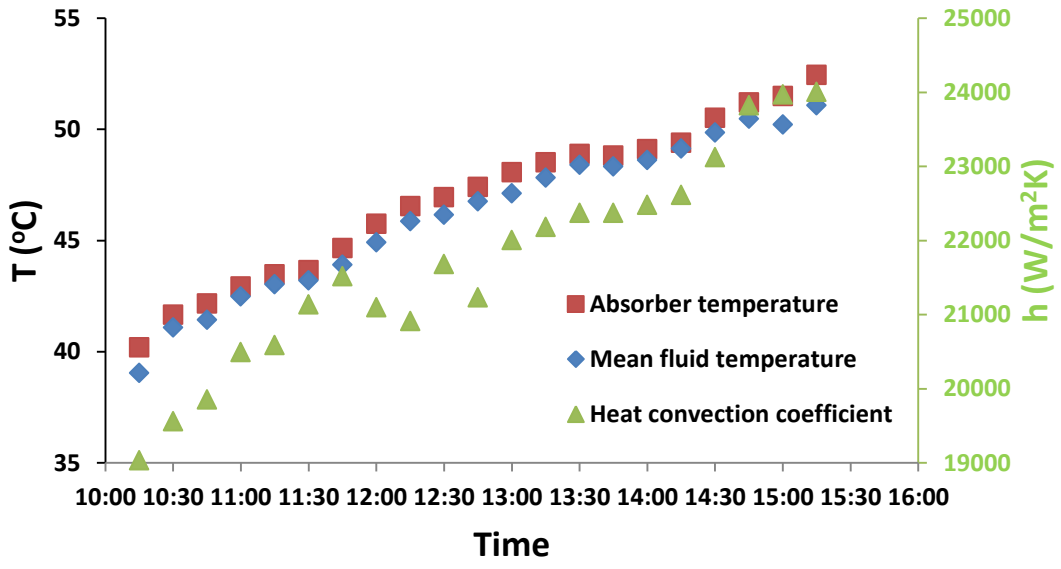

Figure 6. Absorber temperature, fluid temperature and heat transfer coefficient calculated with the numerical model for the examined day

Table 2. Comparison between the experimental and the numerical model results

Measured parameters				Experimental		Numerical		Deviation	
Time (hr)	V (l/h)	T_{in} (°C)	G_b (W/m^2)	T_{out} (°C)	η_{th} -	T_{out} (°C)	n_{th} -	T_{out} -	η_{th} -
10:15	194	33.22	830	44.87	0.3073	46.20	0.3428	2.96%	11.57%
10:30	194	34.63	840	47.53	0.3362	47.73	0.3419	0.42%	1.70%
10:45	195	35.13	845	47.72	0.3278	48.23	0.3417	1.07%	4.23%
11:00	198	36.00	848	48.98	0.3420	48.93	0.3412	0.10%	0.23%
11:15	197	36.51	850	49.54	0.3408	49.52	0.3408	0.04%	0.01%
11:30	201	36.85	849	49.56	0.3395	49.58	0.3407	0.04%	0.34%
11:45	201	37.79	858	50.03	0.3236	50.64	0.3402	1.22%	5.14%
12:00	194	38.61	862	51.21	0.3200	51.98	0.3401	1.50%	6.29%
12:15	190	39.24	865	52.49	0.3284	52.92	0.3396	0.82%	3.41%
12:30	195	39.80	869	52.51	0.3218	53.18	0.3394	1.28%	5.46%
12:45	190	40.06	871	53.47	0.3301	53.84	0.3398	0.69%	2.94%
13:00	194	40.88	873	53.37	0.3132	54.37	0.3387	1.87%	8.15%
13:15	194	41.31	876	54.34	0.3256	54.86	0.3391	0.96%	4.14%
13:30	194	41.78	865	55.02	0.3351	55.14	0.3387	0.22%	1.08%
13:45	194	41.78	857	54.87	0.3344	55.02	0.3387	0.27%	1.30%
14:00	194	42.05	859	55.18	0.3346	55.31	0.3385	0.24%	1.16%
14:15	194	42.37	855	55.91	0.3467	55.56	0.3383	0.63%	2.41%
14:30	194	43.61	845	56.11	0.3238	56.61	0.3374	0.89%	4.19%
14:45	197	44.43	846	56.52	0.3177	57.21	0.3363	1.22%	5.86%
15:00	197	44.77	839	55.66	0.2885	57.43	0.3360	3.18%	16.45%
15:15	194	45.71	830	56.46	0.2835	58.40	0.3352	3.44%	18.23%

5.2 Working fluid investigation

The validated model was used for parametric analysis because of its accuracy and low computational cost. The thermal and exergetic performances were estimated for three working fluids.

Figures 7 and 8 illustrate the thermal and exergetic efficiencies of the collector with water as working fluid. In order to keep the water in its liquid phase, the maximum inlet temperature investigated was 85 ^{o}C. Results show that higher flow rates lead to higher thermal efficiency (Figure 7), but lower exergetic efficiency (Figure 8). The optimum flow rate can be found where both thermal and exergetic efficiencies are satisfying. Thus, the flow rate of 200 l/h was selected as the most appropriate. It is interesting to note that the experimental flow rate was selected close to this value (see Table 2), which shows that the experimental investigation of the collector was performed with approximately the optimum volumetric flow rate.

Figures 9 and 10 show the thermal and exergetic efficiency, respectively, for Therminol VP-1. Thermal efficiency increases with increasing flow rate (Figure 9), while the maximum exergetic efficiency is determined by both the inlet fluid temperature and its flow rate (Figure 10). The average flow rate of 200 l/h offers a reasonable compromise. According to Equation 26, when the oil inlet temperature is close to 155 ^{o}C, maximum exergetic efficiency of approximately 7.58% is observed for all the volumetric flow rates (Figure 10). Table 3 shows the optimum inlet temperatures for the examined flow rates. For each case, the maximum exergetic efficiency is also given. Table 3 shows that higher flow rate leads to higher exergetic efficiency. Moreover, the optimum inlet temperature ranges from 150 ^{o}C to 160 ^{o}C and is generally higher at higher flow rates.

Table 3. Optimum exergetic efficiency with Therminol VP-1 at various flow rates

V (l/h)	$T_{in,opt}$ (^{o}C)	η_{ex} (%)
100	150	7.516
150	155	7.552
200	155	7.570
250	160	7.577
300	160	7.585
350	160	7.590

Consider the useful exergy output as shown in Equation 19 and Equation 20. Higher inlet temperature leads to lower thermal efficiency and to lower useful thermal output (see Figure 9). Since higher inlet temperature leads to a smaller ratio of T_{out}/T_{in} and a higher receiver temperature, it also leads to smaller specific entropy change and thus higher possibility for work. From a mathematical point of view, these contradicting terms allow for an optimum inlet temperature which produces maximum exergetic efficiency, as shown in Figure 10. Similarly, Equation 19 shows that when the receiver temperature decreases from the optimum, the exergetic factor ($1-T_{am}/T_r$) decreases while the useful heat (Q_u) increases, so that the useful exergy output decreases. When the receiver temperature increases from the optimum, the useful exergy output also decreases as the exergetic factor ($1-T_{am}/T_r$) increases and the useful heat (Q_u) decreases. Therefore, an optimum inlet

temperature exists where the best compromise can be made between the exergy supplied and the exergy destroyed.

Figures 11 to 13 depict the results for air as working fluid. Both the thermal (Figure 11) and exergetic efficiency (Figure 12) are very sensitive to flow rate. For exergetic efficiency, the flow rate of 25 l/h is an acceptable compromise. It should be noted that the examined range of air flow rate is much lower than for the other two fluids. Greater air mass flow rates will lead to lower thermal efficiency in the collector and the exergetic efficiency will be very low or negative. Moreover, the exergetic efficiency is very sensitive to mass flow rate due to pressure drop (Figure 13). It is shown that the pressure drop decreases with increasing temperature due to reduced air density.

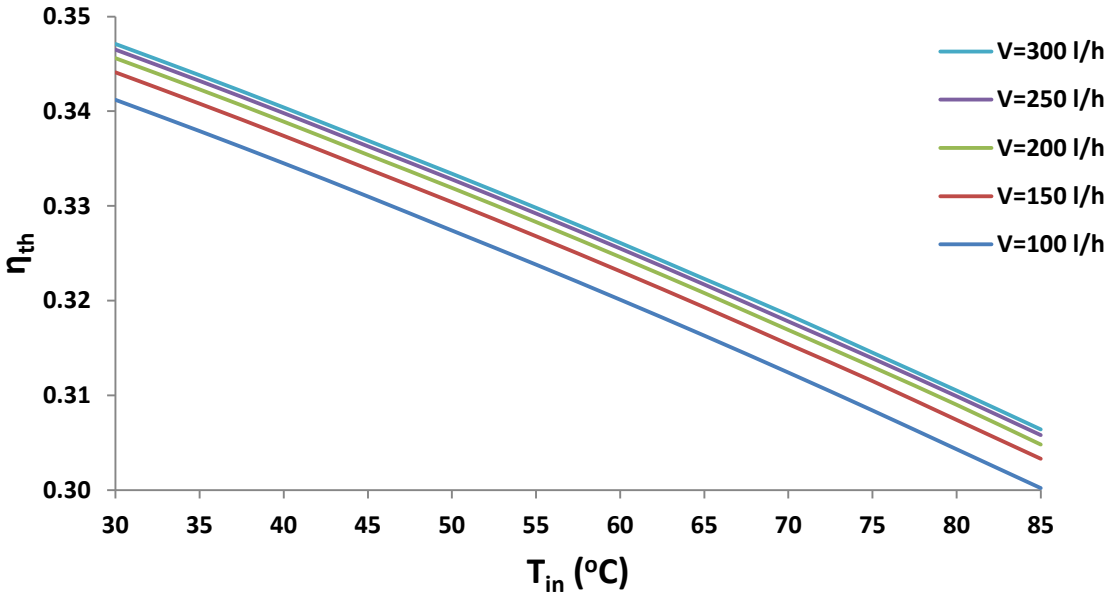

Figure 7. Thermal efficiency for operation with water and various flow rates

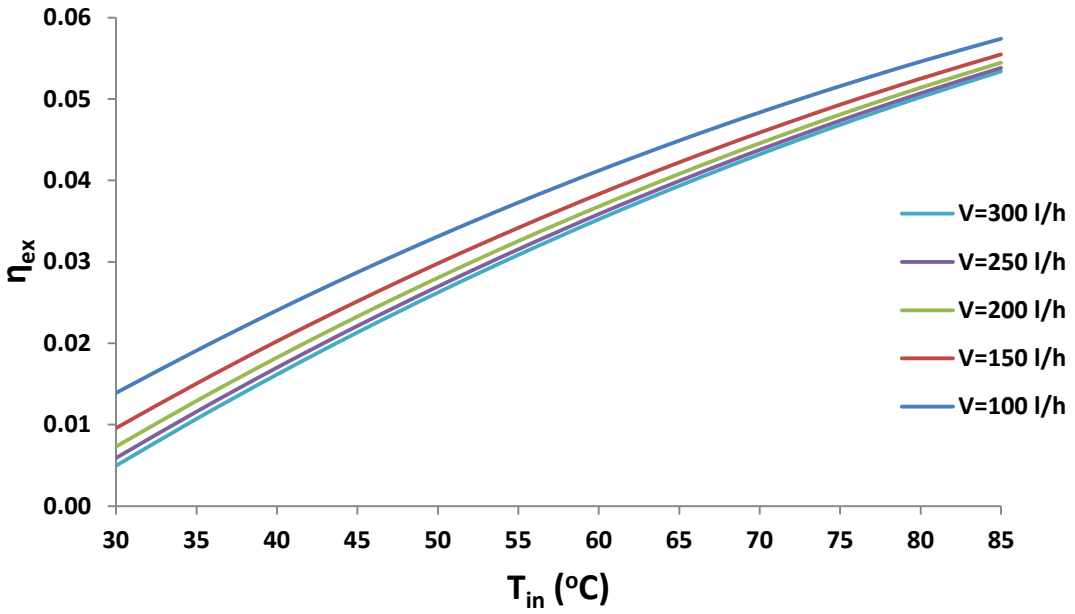

Figure 8. Exergetic efficiency for operation with water and various flow rates

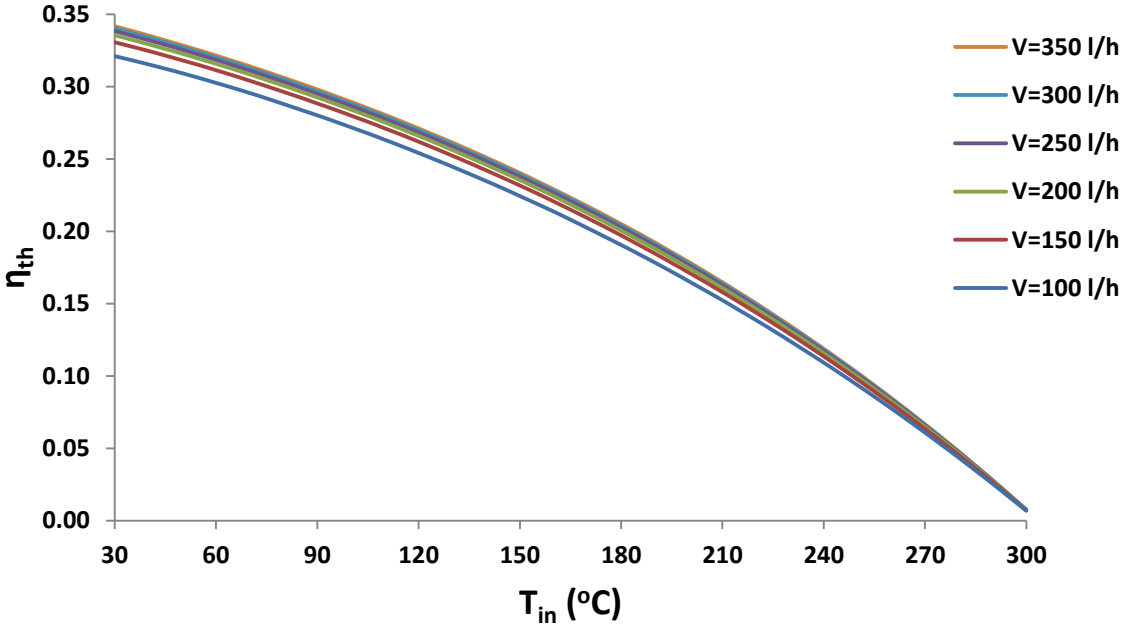

Figure 9. Thermal efficiency for operation with Therminol VP-1 and various flow rates

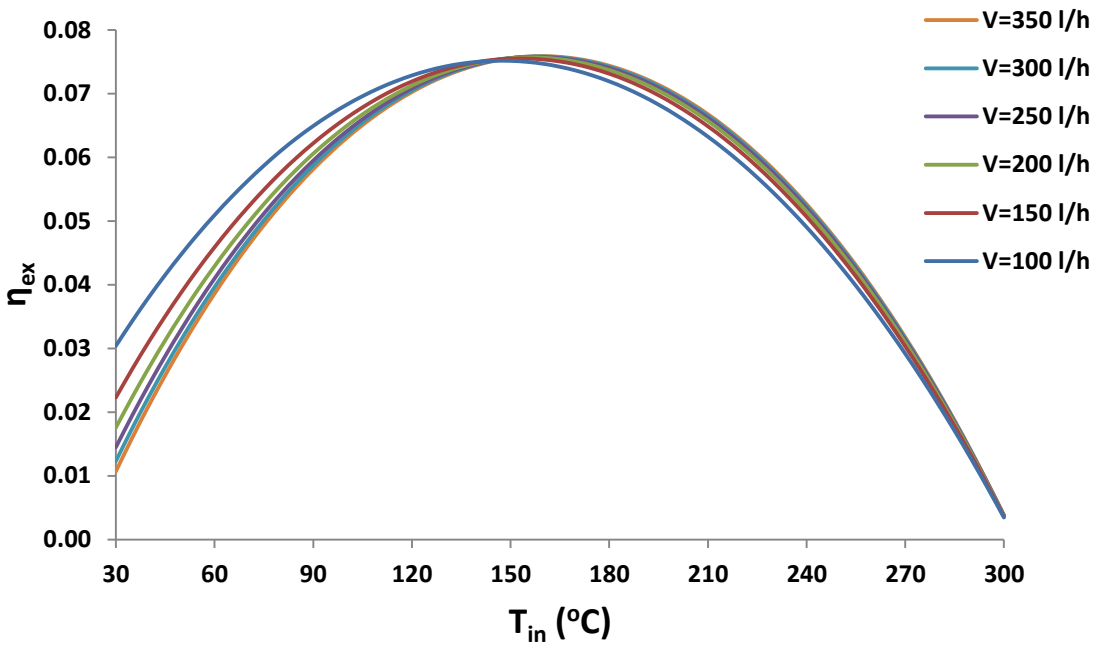

Figure 10. Exergetic efficiency for operation with Therminol VP-1 and various flow rates

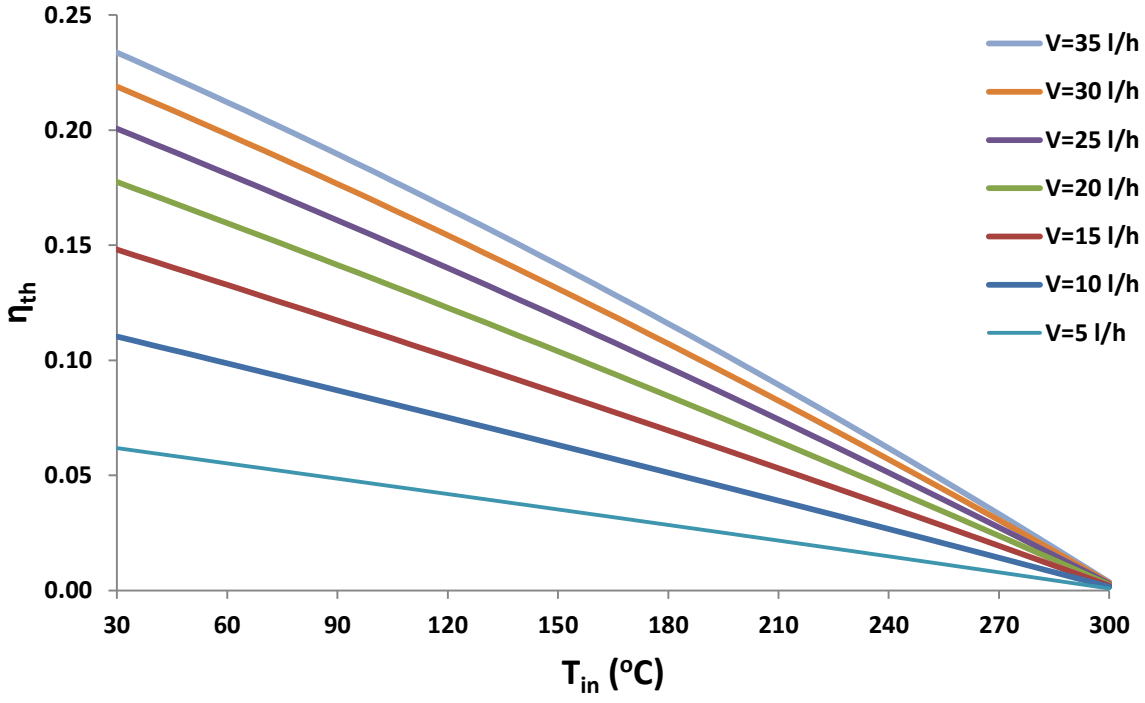

Figure 11. Thermal efficiency for operation with air and various flow rates

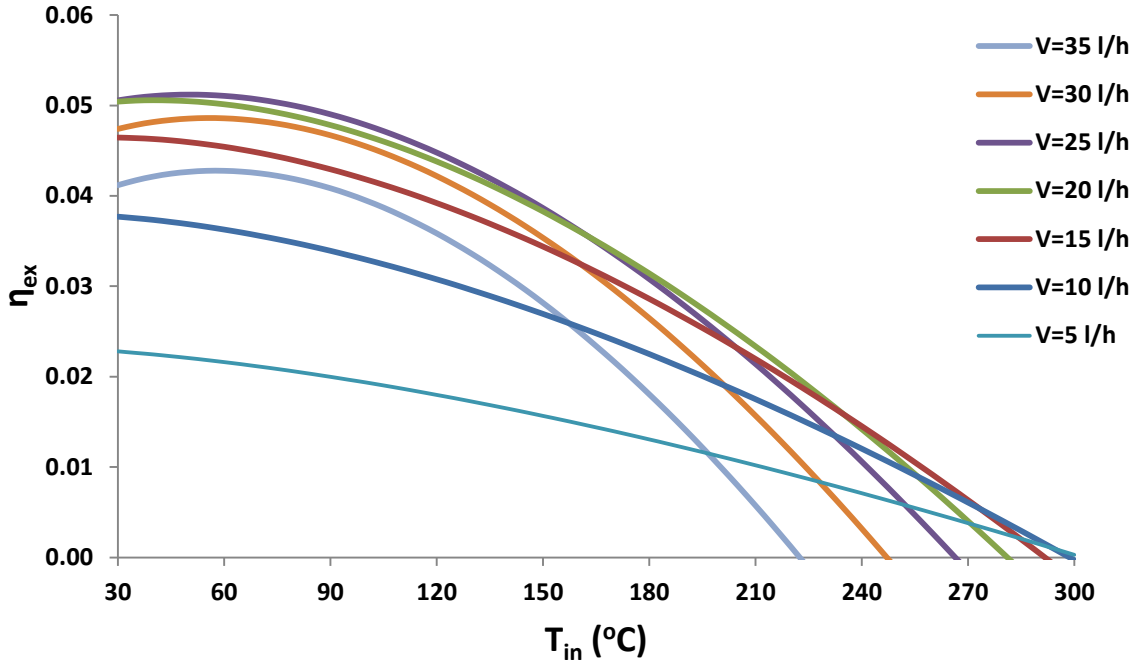

Figure 12. Exergetic efficiency for operation with air and various flow rates

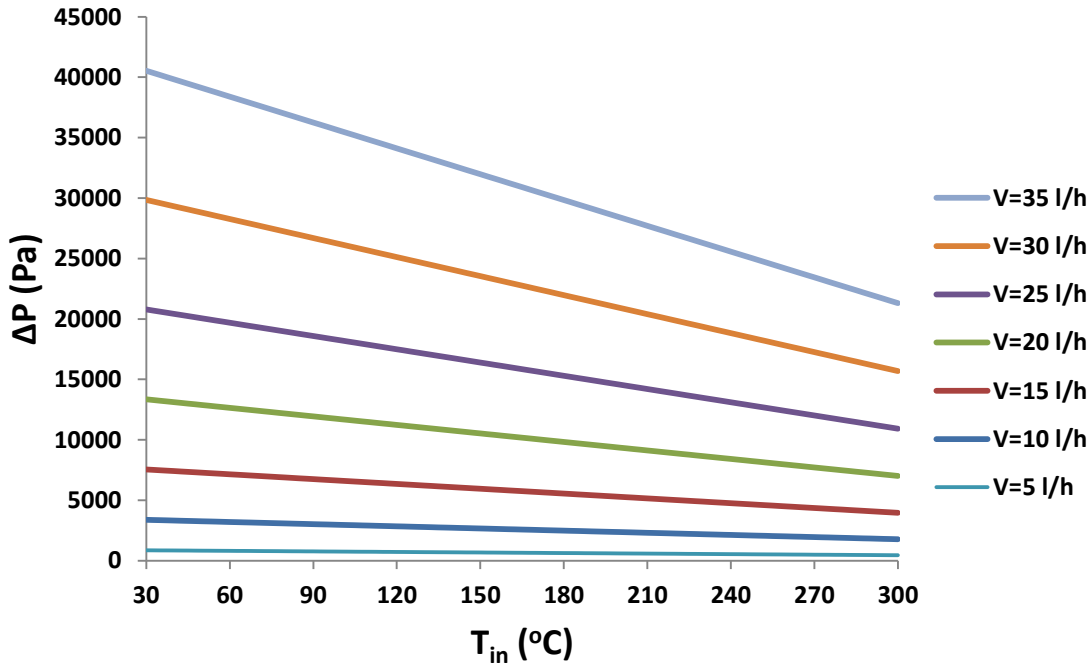

Figure 13. Pressure drop for operation with air and various flow rates

5.3 Comparison of the working fluids

In this section, a comparison of the working fluids is presented. Figure 8 showed that the exergetic efficiency of the collector using water as working fluid increases as the temperature increases. Figures 10 and 12 showed that for Therminol VP-1 and air maximum exergetic efficiencies exist at optimum temperatures and volumetric flow rates. It should be noted that water was only considered in the low-temperature range.

In order to perform a suitable comparison, the optimum volumetric flow rate is selected for each working fluid. Figure 14 shows the thermal comparison of the different working fluids. Water is the best choice for low-temperature applications, while Therminol VP-1 is better for higher-temperature applications. Air is not the best choice in any temperature range. Figure 15 shows the exergetic efficiency for all the working fluids. For low-temperature applications, air is the better fluid exergetically, while for higher-temperature applications, Therminol VP-1 performs better. A maximum exergetic efficiency of 7.58% is achieved with Therminol VP-1 at 155 ^{o}C, as was mentioned in Section 5.2.

The reason for the high exergetic efficiency of the air at low temperatures is the low flow rate which is conjugated with high outlet temperature. This result aids the system to have high exergetic efficiency. At higher temperatures, the low thermal efficiency of the air causes the exergetic efficiency to be reduced significantly, making Therminol VP-1 the better working fluid.

The outlet temperatures of all the working fluids are given in Figure 16. Note that the air outlet temperature curve has a smaller slope compared to the other curves. The receiver performance is given in Figure 17 and the results are similar to Figure 16. Higher receiver temperature leads to higher thermal losses, according to Equations 6-7, and to lower thermal efficiency. Note that this observation is validated by the results of Figure 14. Moreover, by studying Figures 14 and 17 together, the stagnation temperature of the collector can be estimated to be 300 ^{o}C because at this receiver temperature the thermal efficiency is practically zero. Figure 18 shows that the convection heat transfer coefficient is much higher for water. This result is explained by the different thermal properties of the working fluids and it has also been stated in Ref. [34].

The last parameter in the working fluid investigation is the pressure drop, which is shown in Figure 19. The pressure drop is extremely high for air, a result which has also been noticed in the previous section. Therminol VP-1 and water have similar pressure losses because these fluids are both liquids. The results of Figure 19 indicate that pressure loss is a significant factor for evaluating the collector, especially in the case of gas working fluids. The exergetic analysis takes the pressure losses into account and it is the most appropriate index for evaluating the solar collector performance.

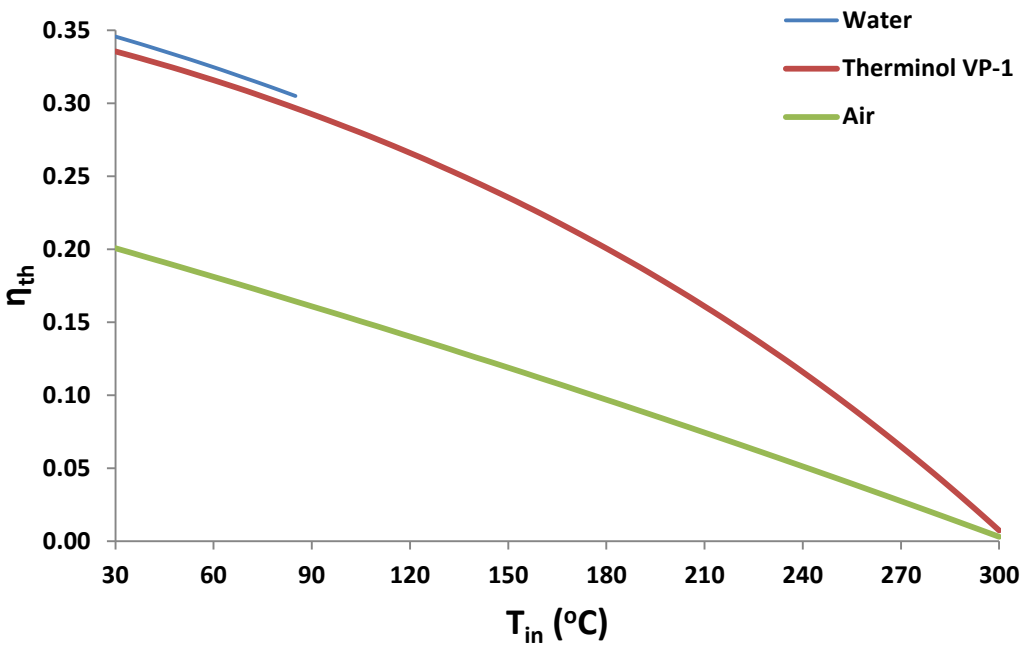

Figure 14. Thermal efficiency comparison among the examined working fluids

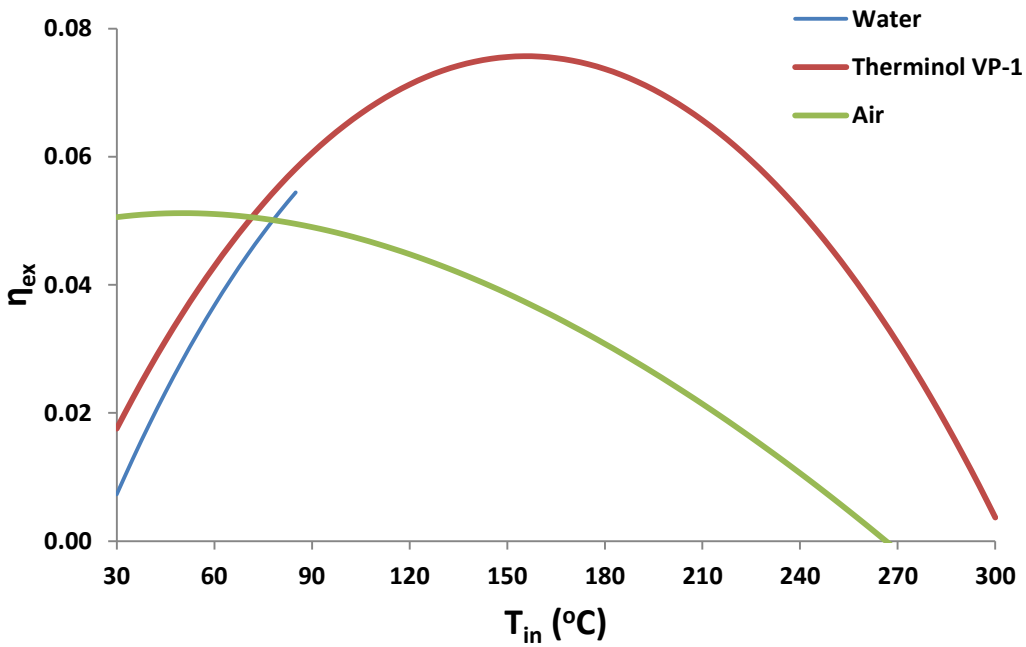

Figure 15. Exergetic efficiency comparison among the examined working fluids

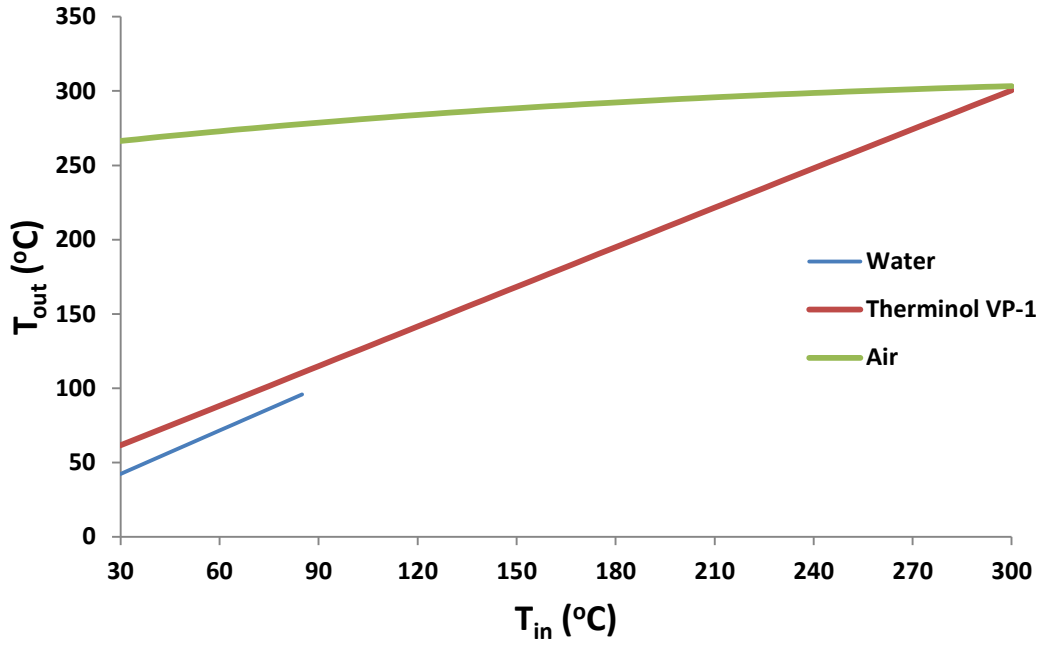

Figure 16. Outlet temperature comparison among the examined working fluids

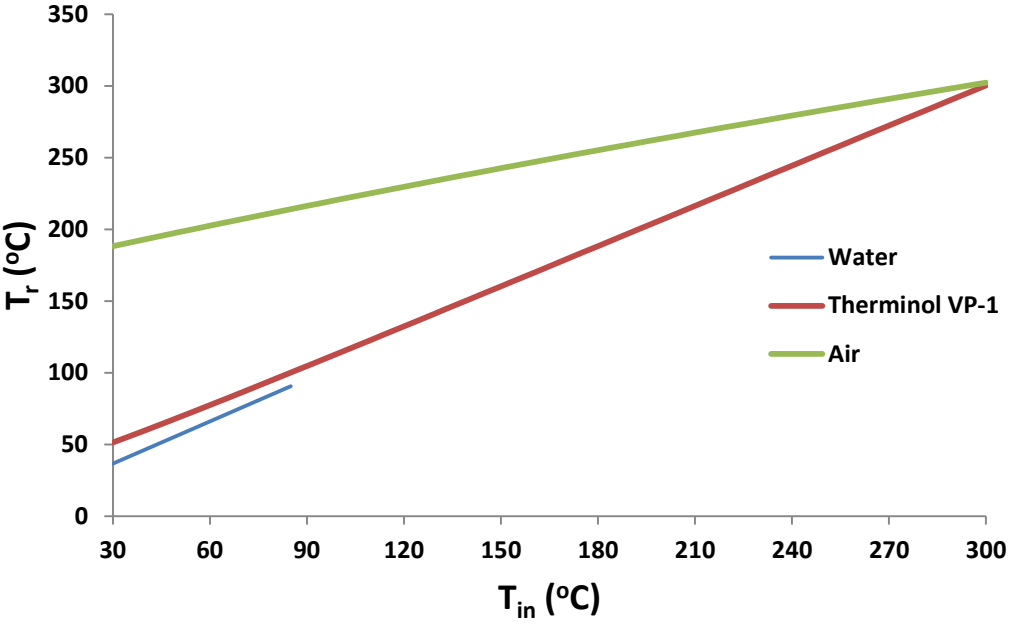

Figure 17. Receiver temperature comparison among the examined working fluids

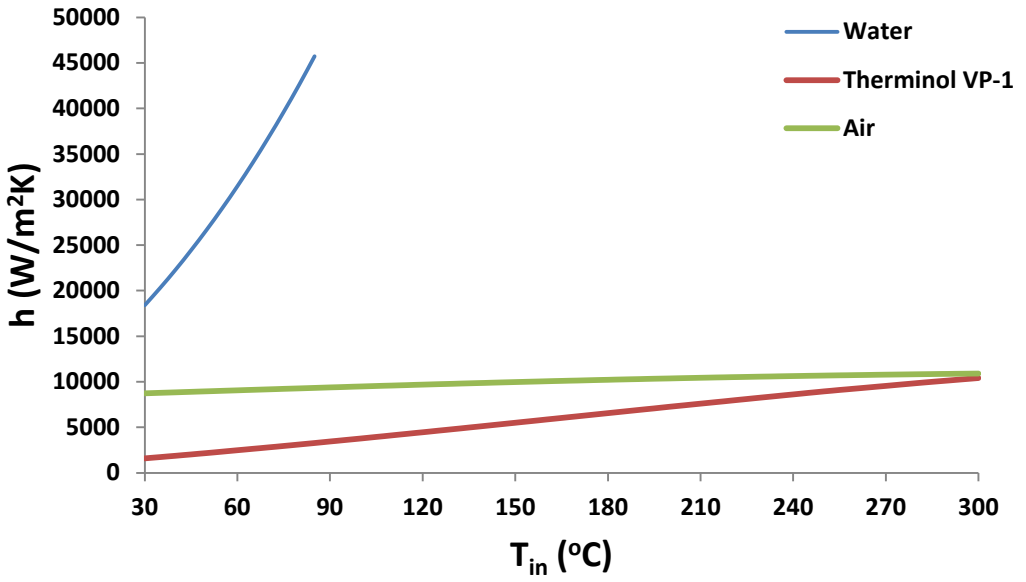

Figure 18. Convection heat transfer coefficient comparison among the examined working fluids

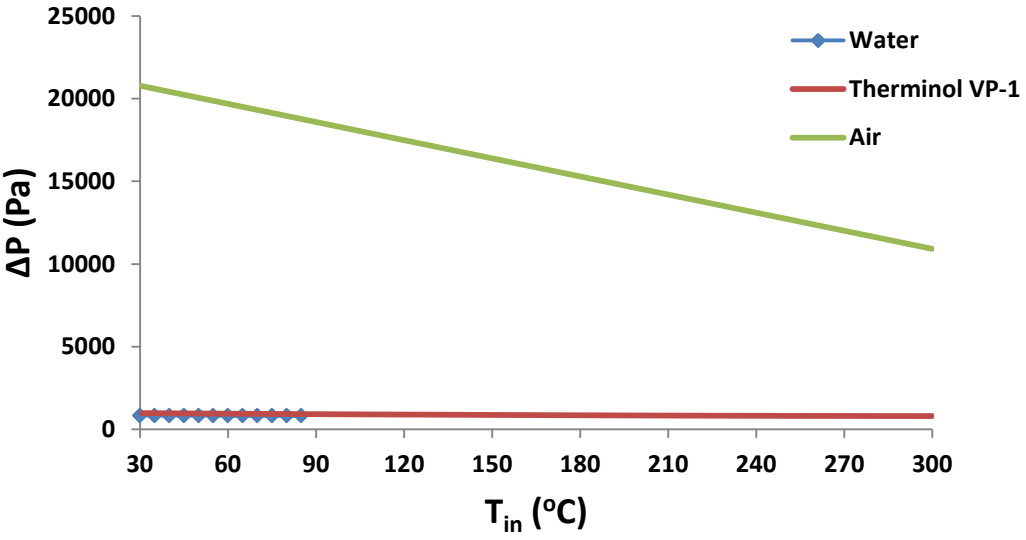

Figure 19. Pressure drop comparison among the examined working fluids

5.4 Energetic and financial evaluation of the examined solar collector

In this section, the experimental solar collector is evaluated in energetic and exergetic terms. The useful heat output rate of the collector for various water inlet temperatures and solar beam irradiation levels is given in Figure 20. Furthermore, the experimental thermal efficiency of the collector is given according to the following equation:

$$\eta_{th} = 0.3446 - 0.4632 \cdot \left(\frac{T_{in} - T_{am}}{G_b} \right), \tag{28}$$

As shown in Figure 20, the useful heat output rate can reach values close to 3500 W. This useful heat output rate can be further increased by eliminating manufacturing errors which are associated with the concentrator geometry. In this analysis, the ambient temperature was assumed to be 20 ^{o}C.

The next step in this investigation is the financial evaluation of the solar collector. Simple payback period (SPP) is a financial index which clearly indicates the feasibility of a system. Different scenarios are examined with two-parametric analysis. More specifically, Figure 21 exhibits the SPP for different combinations of heating cost and yearly solar beam irradiation potential. The formula which calculates the SPP is the following:

$$SPP = \frac{C_0}{A_a \cdot YSP \cdot \eta_{th,m} \cdot K_{heat}}, \tag{29}$$

In Equation 29, the capital cost of the collector (C_0) is equal to 7000 € and a mean thermal efficiency of 31.5% is used by assuming a 70^{o}C inlet temperature. Figure 21 shows that the payback period ranges from less than 4 years to about 15 years. Generally, a payback period of up to 10 years is accepted for renewable energy systems, which means that this system can be feasible in areas with solar potential of more than 1600 kWh/m^2 and where the cost of heating is more than 0.15 €/kWh.

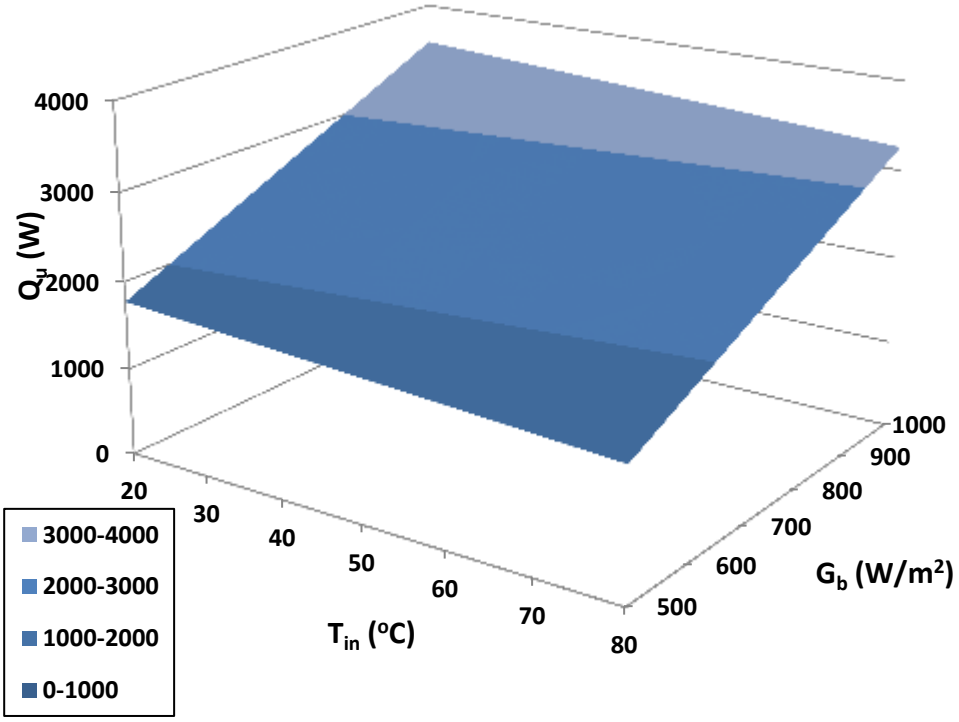

Figure 20. Useful heat production rate of the collector for various operating conditions

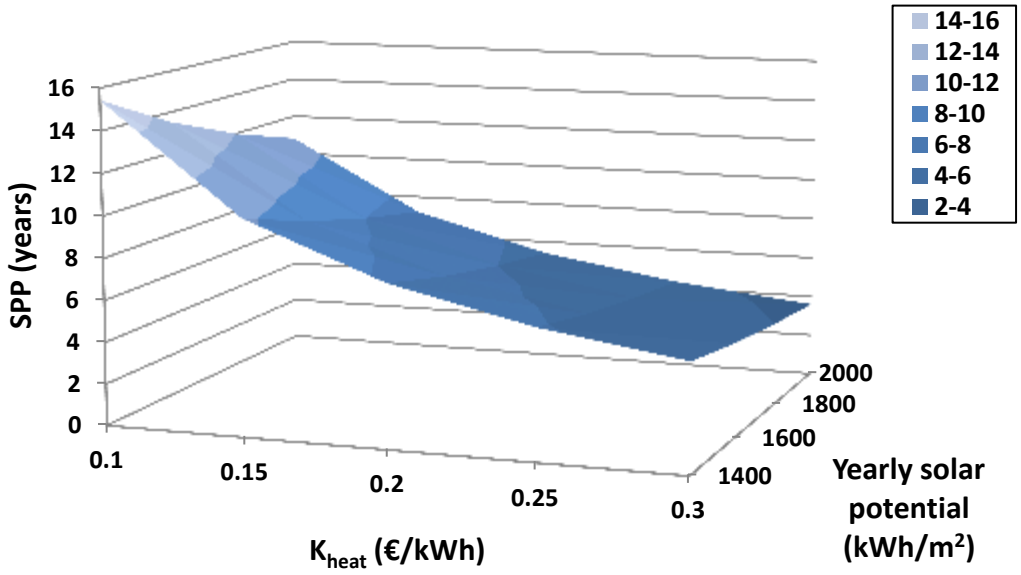

Figure 21. Simple payback period of the collector for different combinations of heating cost and yearly solar potential

6. Conclusion

As a potential alternative to fossil fuels, solar-tracking dish collectors are able to produce heat at high temperatures. Important considerations for solar collectors are manufacturing costs, complexity, efficiency, uniform flux distribution and working fluid selection. In this work, a simple, low-cost solar collector with dish reflector and spiral absorber was investigated experimentally and numerically.

In the experimental study, the solar-tracking dish collector was connected to a water storage tank of 500 litres. The following parameters were measured: the volumetric water flow rate, the water inlet temperature, the water outlet temperature, the ambient temperature, the air velocity and the solar beam irradiance. Experimental results were used to validate a numerical model developed in Engineering Equation Solver. Apart from heating water, the collector can also be utilized for higher-temperature applications of over 100 ^{o}C and therefore two other common working fluids (thermal oil and air) were also investigated at various operating conditions, using the validated numerical model.

The thermal efficiency of the collector was found to be around 34% according to experimental results with water as working fluid. This low thermal efficiency can be explained by the low optical efficiency of the collector. The low-cost materials lead to manufacturing errors in the concentrator geometry, which lead to a relatively low intercept factor. Moreover, a relatively low reflectance due to dust and stains was an extra contributor to the low performance of the collector.

The thermal efficiency comparison of the working fluids suggests that water is the best working fluid, followed by thermal oil, while air is the least efficient working fluid. Moreover, it is essential to state that the pressure losses are significantly higher for air and

that this has been taken into account in the exergetic analysis. The optimum exergetic efficiency was observed for thermal oil as working fluid with inlet temperature of 155^{o}C. Furthermore, the exergetic analysis showed that air is a promising working fluid in low-temperature applications because of its high outlet temperature. This result shows that for applications where the ambient air is directly heated without a storage system, the configuration does not only have a lower cost, but the exergetic output is also high.

For future work, the present collector can be examined experimentally at higher temperatures with thermal oil and air as working fluid. The experimental results will determine the exact performance of the present system in all the examined conditions. Moreover, the geometry of the reflector can be improved significantly to minimize manufacturing errors, improve efficiency and decrease the simple payback period. The system in its current state can be feasible in areas with solar potential of more than 1600 kWh/m^2 and where the cost of heating is more than 0.15 €/kWh.

Acknowledgements

This paper is included in the research framework of Research Project: III42006 – Research and Development of Energy and Environmentally Highly Effective Polygeneration Systems Based on Renewable Energy Resources. This project is financed by the Ministry of Education, Science and Technological Development of the Republic of Serbia.

Nomenclature

A Area, m^2

C Concentration ratio, -

C_0 Capital cost of the collector, €

c_p Specific heat capacity under constant pressure, J/kg K

D Diameter, m

E Exergy flow rate, W

f_r Friction factor, -

G Global solar irradiation, W/m^2

G_b Solar beam irradiation, W/m^2

G_d Solar diffuse irradiation, W/m^2

h Convection heat transfer coefficient, W/m^{2}K

h_{air} Convection heat transfer coefficient between absorber and ambient air, W/m^{2}K

k Thermal conductivity, W/mK

K_{heat} Cost of the produced useful heat, €/kWh

L Tube length, mm

m Mass flow rate, kg/s

Nu Mean Nusselt number, -

Pr Prandtl number, -

Q Heat transfer rate, W

Re Reynolds number, -

SPP Simple payback period, years

T Temperature, K

u Working fluid velocity, m/s

V Volumetric flow rate, l/h

V_{air} Ambient air velocity, m/s

YSP Yearly solar beam irradiation potential, kWh/m^2

Greek symbols

α Absorbance, -

γ Intercept factor, -

ΔP Pressure drop, Pa

Δs Specific entropy increase, J/kg K

ε Emittance, -

η Efficiency, -

μ Dynamic viscosity, Pa s

ρ Density, kg/m^3

ρ_c Concentrator reflectance, -

σ Stefan–Boltzmann constant [= $5.67 \cdot 10^{-8}$ W/m^2 K^4]

Subscripts and superscripts

a aperture

abs	absorbed
am	ambient
conv	convection
ex	exergetic
fm	mean fluid
in	inlet
in,opt	inlet optimum
m	mean
loss	losses
opt	optical
out	outlet
r	receiver
rad	radiation
ri	inner receiver
ri,min	inner receiver minimum
ro	outer receiver
s	solar
sun	sun
th	thermal
u	useful

Abbreviations

EES Engineering Equator Solver

PMMA Polymethyl methacrylate

References

[1] C. Tzivanidis, E. Bellos, G. Mitsopoulos, et al., Energetic and financial evaluation of a solar assisted heat pump heating system with other usual heating systems in Athens, Appl. Therm. Eng. 2016;106:87-97

[2] P. Iodice, M. Dentice d'Accadia, C. Abagnale, et al., Energy, economic and environmental performance appraisal of a trigeneration power plant for a new district: Advantages of using a renewable fuel, Appl. Therm. Eng. 2016;95:330-338

[3] E. Gholamian, S.M.S. Mahmoudi, V. Zare, Proposal, exergy analysis and optimization of a new biomass-based cogeneration system, Appl. Therm. Eng. 2016;93:223-235

[4] H. Li, X. Zhang, L. Liu, et al., Exergy and environmental assessments of a novel trigeneration system taking biomass and solar energy as co-feeds, Appl. Therm. Eng. 2016;104:697-706

[5] BP Statistical Review of World Energy, June 2015

[6] M. Valipour, Future of agricultural water management in Africa, Arch. Agron. Soil Sci. 2015, 61(7);907-927

[7] M. Valipour, V.P. Singh, Global Experiences on Wastewater Irrigation: Challenges and Prospects, in Book: Balanced Urban Development: Options and Strategies for Liveable Cities, Springer open 2016;72:289-328

[8] E. Bellos, C. Tzivanidis, K.A. Antonopoulos, Exergetic, energetic and financial evaluation of a solar driven absorption cooling system with various collector types, Appl. Therm. Eng. 2016;102:749-759

[9] M. Valipour, Optimization of neural networks for precipitation analysis in a humid region to detect drought and wet year alarms 2016; Meteorol. Appl.;23:91–100

[10] M. Valipour, S. Eslamian, Analysis of potential evapotranspiration using 11 modified temperature-based models, Int. J. Hydrol. Sci. Technol. 2014;4(3):192-207

[11] E. Bellos, D. Korres, C. Tzivanidis, et al., Design, simulation and optimization of a compound parabolic collector, Sustain. Energy Technol. Assess. 2016;16:53-63

[12] S.A. Kalogirou, Solar thermal collectors and applications, Progress Energ. Comb. 2004;30:231–295

[13] L. Zhou, Y. Li, E. Hu, et al., Comparison in net solar efficiency between the use of concentrating and non-concentrating solar collectors in solar aided power generation systems, Appl. Therm. Eng. 2015;75:685-691

[14] M. Abid, T. A. H. Ratlamwala, U. Atikol, Performance assessment of parabolic dish and parabolic trough solar thermal power plant using nanofluids and molten salts, Int. J. Energy Res. 2016; 40:550–563

[15] W.G. Le Roux, T. Bello-Ochende, J.P. Meyer, The efficiency of an open-cavity tubular solar receiver for a small-scale solar thermal Brayton cycle, Energ. Convers. Manage. 2014; 84:457-470.

[16] R. Loni, A.B. Kasaeian, E. Askari Asli-Ardeh, et al., Optimizing the efficiency of a solar receiver with tubular cylindrical cavity for a solar-powered organic Rankine cycle, Energy 2016;112:1259-1272

[17] R. Loni, A.B. Kasaeian, E. Askari Asli-Ardeh, et al., Performance study of a solar-assisted organic Rankine cycle using a dish-mounted rectangular-cavity tubular solar receiver, Appl. Therm. Eng. 2016; 108:1298-1309.

[18] G. Xiao, T. Yang, D. Ni, et al., A model-based approach for optical performance assessment and optimization of a solar dish, Rene. Energ. 2017; 100(C): 103-113.

[19] Z. Li, D. Tang, J. Du, et al., Study on the radiation flux and temperature distributions of the concentrator–receiver system in a solar dish/Stirling power facility, Appl. Therm. Eng. 2011;31(10):1780-1789

[20] Z.M. Omara, Mohamed A. Eltawil, Hybrid of solar dish concentrator, new boiler and simple solar collector for brackish water desalination, Desalination 2013;326:62-68

[21] G.O. Prado, L.G. M.Vieira, J.J.R. Damasceno, Solar dish concentrator for desalting water, Sol. Energy 2016;136:659-667

[22] A.M. Daabo, S. Mahmoud, R.K. Al-Dadah, The effect of receiver geometry on the optical performance of a small-scale solar cavity receiver for parabolic dish applications, Energy 2016;114:513-525

[23] J. Zhu, K. Wang, G. Li, et al., Experimental study of the energy and exergy performance for a pressurized volumetric solar receiver, Appl. Therm. Eng. 2016;104:212-221

[24] S.R. Pavlović, E. Bellos, V.P. Stefanović, et al., Design, simulation and optimization of a solar dish collector spiral-coil thermal absorber, Therm. Sci. 2016; 20: 1387-1397

[25] J.A. Duffie, W.A. Beckman, Solar Engineering of Thermal Processes, 3rd edition, Wiley, Hoboken, NJ, USA, 2006

[26] J. Leinhard IV, J. Leinhard V, A Heat Tranfer Textbook, 4th edition, Phlogiston Press, USA, 2012, 354–360

[27] M.L. Djordevic, V.P. Stefanovic, M.V. Mancic, Pressure drop and stability of flow in Archimedean spiral tube with transverse corrugations, Therm. Sci. 2016;20(2):579-591

[28] E. Bellos, C. Tzivanidis, K.A. Antonopoulos, et al., The use of gas working fluids in parabolic trough collectors – An energetic and exergetic analysis, Appl. Therm. Eng. 2016;109(A):1-14

[29] E. Bellos, C. Tzivanidis, K.A. Antonopoulos, et. al, Thermal enhancement of solar parabolic trough collectors by using nanofluids and converging-diverging absorber tube, Rene. Energ. 2016;94:213-222

[30] F-Chart Software, Engineering Equation Solver (EES); 2015. Available at: http://www. fchart.com/ees.

[31] Electrical Research Association, 1967 Steam Tables, Thermodynamic Properties of Water and Steam; Viscosity of Water and Steam, Thermal Conductivity of Water and Steam, Edward Arnold Publishers, London, 1967.

[32] Therminol, Therminol VP-1; 2016. Available at: http://www.therminol.com/pages/bulletins/therminol_VP1.pdf.

[33] E.W. Lemmon, R.T. Jacobsen, S.G. Penoncello, et al., Thermodynamic Properties of Air and Mixtures of Nitrogen, Argon, and Oxygen from 60 to 2000 K at Pressures to 2000 MPa, J.Phys.Chem. Ref. Data 2000;29(3)

[34] E. Bellos, C. Tzivanidis, K.A. Antonopoulos, A detailed working fluid investigation for solar parabolic trough collectors, Appl. Therm. Eng. 2017;114(5):374-386